Fermi Surface Nesting and Structural Transition on a Metal Surface: In/Cu(001)

T. Nakagawa,[1] G. I. Boishin,[1,*] H. Fujioka,[1] H. W. Yeom,[2] I. Matsuda,[3] N. Takagi,[1,†] M. Nishijima,[1] and T. Aruga[1,‡]

[1]*Department of Chemistry, Graduate School of Science, Kyoto University, Kyoto 606-8502, Japan*

[2]*Atomic-Scale Surface Science Research Center and Institute of Physics and Applied Physics, Yonsei University, Seoul 120-749, Korea*

[3]*Department of Chemistry, The University of Tokyo, Tokyo 113-0033, Japan*

(Received 15 February 2000)

Peierls-type instability and structural phase transition are shown to occur on the surface of a normal metal. An In overlayer on Cu(001) undergoes a reversible transition at ~350 K. Scanning tunneling microscopy of the low-temperature, reduced-symmetry phase indicates a strong periodic lattice distortion (PLD). Angle-resolved photoemission of the high-temperature phase reveals that the In-derived surface resonance constitutes a square-shaped, quasi-two-dimensional Fermi surface within the projected bulk Cu bands. The Fermi surface exhibits one-dimensional nesting upon the transition, which is in agreement with the PLD periodicity.

DOI: 10.1103/PhysRevLett.86.854 PACS numbers: 71.18.+y, 68.35.Bs, 71.45.Lr, 73.20.At

Phase transitions in reduced dimensional materials are important to understand fundamental problems in solid state physics. Because of the simple Fermi surface (FS) in reduced dimensions, electrons near the Fermi level are unstable against a lattice distortion. This instability leads the materials to a phase transition at a finite temperature and a reduced-symmetry ground state appears at low temperature (LT) [1]. The Peierls transition is a manifestation of such instability, which is expected for one-dimensional (1D) electron systems interacting with phonons at $2k_F$, where k_F refers to the Fermi wave vector [2]. In the Peierls transition, the FS nesting manifests itself as periodic lattice distortion (PLD) and charge density wave (CDW). Some bulk materials with anisotropic crystal structures, such as transition metal chalcogenides, transition metal bronzes, and organic molecular crystals, are known to undergo the Peierls transition [1].

Solid surface is a seemingly suitable candidate for the study of the physics in reduced dimensions. However, there are only a few surfaces which invoke surface-intrinsic Peierls transitions or CDWs. The reconstruction of low-index, clean and hydrogen-covered surfaces of Mo and W has been investigated for a long time [3]. The Peierls instability has been discussed as a driving mechanism for the reconstruction, but it is still under controversy [4–6]. While the origin of the phase transition of Pb(Sn)/Ge(111) [7,8] was first suggested to be surface CDW, other scenarios such as order-disorder transition [9] and the Jahn-Teller-like instability based on a local bonding of surface states [10] are also proposed. Recently metallic linear chains of In on Si(111) are shown to undergo a CDW transition [11]. The nesting of the quasi-1D FS of the Si(111)-(4×1)-In phase, within the bulk band gap, is shown to drive the transition. So far no surface CDWs have been evidenced on metal surfaces.

In this Letter we present experimental evidence for the FS nesting and instability in a metallic ultrathin film of In adsorbed on Cu(001). We observed by low-energy electron diffraction (LEED) that In/Cu(100) with 1 monolayer (ML) coverage of In [1 ML is defined as the atom density of Cu(001), 1.53×10^{19} m^{-2}] undergoes a reversible transition between high-temperature (HT) $c(2 \times 2)$ and LT $(9\sqrt{2} \times 2\sqrt{2})R45°$ phases at ~350 K. Scanning tunneling microscopy (STM) of the LT phase shows a local atomic arrangement similar to the HT phase but with a strong PLD. Using angle-resolved photoelectron spectroscopy (ARPES), we find a surface resonance for $c(2 \times 2)$-In, which disperses within the projected bulk Cu bands and constitutes a square shape FS around $\bar{\Gamma}'$. It is shown that the reciprocal lattice vector, Q, of $(9\sqrt{2} \times 2\sqrt{2})R45°$ and $2k_F$ of the $c(2 \times 2)$ phase are closely commensurable. In the LT phase, the surface resonance band exhibits a band gap, whose largest magnitude is 400 meV relative to E_F.

All the STM images shown below were taken with a variable temperature STM (Oxford Instruments) in the constant-current (topographic) mode. The ARPES experiments were done with an ADES-500 (VG Microtech) spectrometer at the beam line 7B of Photon Factory. Some experiments were done with an ARUPS-10 (VG Microtech) spectrometer and unpolarized He-II radiation (40.8 eV). In both ARPES experiments the total energy resolution deduced from the width of the Fermi edge was 150 meV and the acceptance angle was 1°. The experimental uncertainty of the measured Fermi wave vectors was 0.03 Å^{-1}. The Cu sample was cleaned by repeated cycles of Ar ion sputtering and annealing at 770 K. The cleanness of the sample was checked by Auger electron spectroscopy (AES), ARPES observation of the Cu(001) surface states [12,13], and observation of the sharp LEED patterns of the clean and In-covered surfaces. In was evaporated from a crucible with the sample kept at room temperature. The In coverage was monitored and calibrated by the combination of AES, LEED, and work function measurements [14]. AES intensities of Cu and In show a series of simultaneous breaks as a function of deposition time. The $(9\sqrt{2} \times 2\sqrt{2})R45°$ pattern [Fig. 1(b)]

 0031-9007/01/86(5)/854(4)$15.00

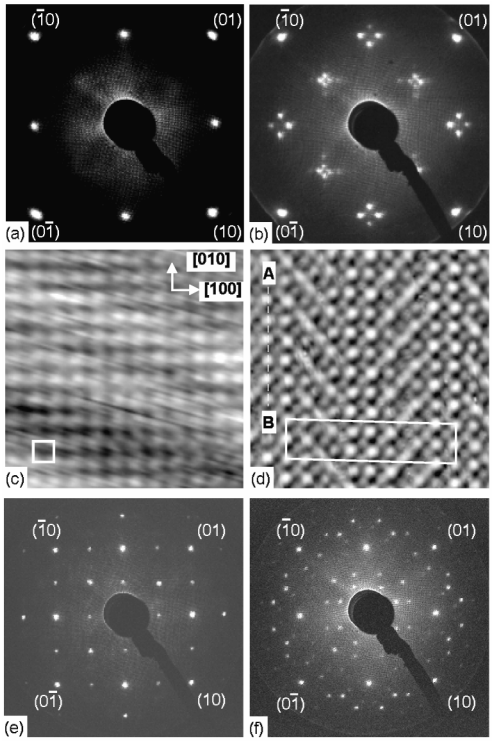

FIG. 1. LEED patterns of (a) HT ($T = 420$ K) and (b) LT ($T = 110$ K) phases at $\theta_{\mathrm{In}} = 1.0$ ML at the incident energy, E_p, of 60 eV. STM images of (c) the HT phase ($T = 420$ K) acquired with the sample bias $V_s = -20$ mV and tunneling current $I_t = 4$ nA and (d) the LT phase ($T = 300$ K) acquired with $V_s = -5$ mV and $I_t = 4$ nA. The scan area of both images is 40×40 Å^2 and the orientation is the same. Also shown are the LEED patterns taken at 110 K for (e) $\theta_{\mathrm{In}} \sim 1.3$ ML ($E_p = 114$ eV) and (f) $\theta_{\mathrm{In}} \sim 2.0$ ML ($E_p = 125$ eV).

is sharply observed at around the first break, which was assumed to be corresponding to 1.0 ML based on the attenuation of the Cu Auger signal and STM images of this surface. Upon further deposition, $c(4 \times 4)$ [Fig. 1(e)] and $(\sqrt{10} \times \sqrt{10})R18.4° + (2 \times 2)$ [Fig. 1(f)] patterns are successively observed at around $\theta_{\mathrm{In}} \sim 1.3$ and 2.0 ML, respectively [14]. For the ARPES experiment shown below, the coverage was controlled within a relative error of ± 0.05 ML by monitoring work function, and sharp and well-contrasted LEED patterns were verified before and after every series of measurements.

In the LEED pattern of $(9\sqrt{2} \times 2\sqrt{2})R45°$ [Fig. 1(b)], sharp 1/18th order spots are observed around half order positions. Note that the $(1/2, 1/2)$ spots are missing. This phase is stable down to the 110 K studied. Upon heating, the surface undergoes a reversible phase transition at $T_c \sim 350$ K to a HT phase which exhibits a high-symmetry, $c(2 \times 2)$ LEED pattern [Fig. 1(a)]. AES intensities of In and Cu were found to be constant during the transition, which suggests that no mass transfer of both In and Cu atoms normal to the surface is associated with the transition.

In Fig. 1 we also present topographic STM images for the HT and LT phases at $\theta_{\mathrm{In}} = 1.0$. The STM image of the HT phase consists of a square unit cell with its sides aligned along [100] and the periodicity $a_0 = 3.6$ Å, as shown by a small square. This unit cell has a $c(2 \times 2)$ $[(\sqrt{2} \times \sqrt{2})R45°]$ symmetry and is consistent with the LEED pattern observed for this surface. Since the metallic radius of In is larger by ~30% than Cu, we suggest that In atoms form a bilayer structure with both layers consisting of 0.5 ML each of In atoms arranged in $c(2 \times 2)$.

With decreasing temperature, this surface changes its translational symmetry and a uniaxial PLD is observed as shown in Fig. 1(d). The average spacing between neighboring protrusions is ~2.6 Å, which is comparable to that on Cu(001). The protrusions of the STM image are not equivalent. The apparent height difference between strong and weak protrusions is ~0.1 Å, which represents a spatial profile of the density of surface electronic states and implies a rumpling of the surface atoms.

The LT phase has $9a_0$ and $2a_0$ periodicity in [100] and [010], respectively, giving rise to a $(9\sqrt{2} \times 2\sqrt{2})R45°$ unit cell, in agreement with the LEED result. The stripes of apparently $c(2 \times 2)$ domains along the line A-B are separated by herringbonelike intermediate domains. The neighboring $c(2 \times 2)$-like domains are in antiphase relation, which makes the $(1/2, 1/2)$ LEED spots missing. A close look at the STM image shows that there is also a lateral deformation as seen along the line A-B in Fig. 1(d). The Fourier transform of the STM image is identical with the observed LEED pattern, except that the LEED pattern consists of contributions from two equivalent domains rotated by 90° with each other. The wider STM scans showed that the surface is covered with a flat, uniform In layer and the domain size is limited by the terrace width of the substrate (~500 Å).

We measured ARPES spectra of the Cu(001)-$c(2 \times 2)$-In over a wide range of the surface Brillouin zone (SBZ). We first summarize the valence band structure of the HT and LT phases in Fig. 2(a). The shaded area indicates the bulk Cu bands projected onto the Cu(001)-(1×1) surface [15]. An In-induced band, S, is observed near E_F. We checked that S is not observed for clean Cu(100) under the same condition. The surface umklapp process on $c(2 \times 2)$ or $(9\sqrt{2} \times 2\sqrt{2})R45°$ does not account for the S peak. The surface origin of the S peak was also certified by checking that the 2D band dispersion is not influenced by varying photon energies between 18 and 27 eV. The S band is a surface localized state and its origin is ascribed to an In $5sp$-Cu $4sp$ derived band. The band structure of S is nearly the same in both phases except near E_F.

Figure 2(b) shows a series of photoemission spectra for the HT and LT phases along the $\bar{M}'$-$\bar{\Gamma}'_{10}$ line, taken with linearly polarized 22.8-eV synchrotron radiation which was incident at 45° to the surface normal with photon polarization in a (110) incident plane. The k_x value marked

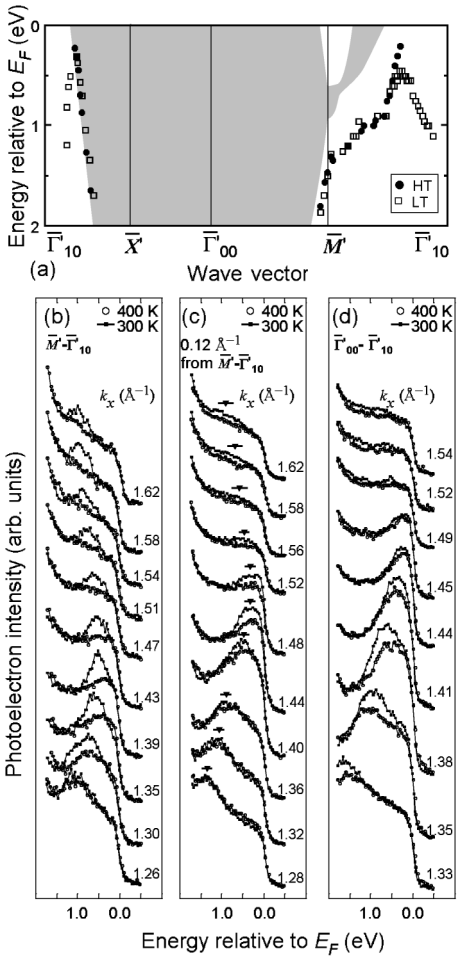

FIG. 2. (a) Valence band structure within 2 eV from E_F (see Fig. 3 for notation). The data obtained with $h\nu = 22.78$ eV are shown. Filled circles are for the HT phase and open squares for the LT phase. Angle-resolved photoelectron spectra for HT ($T = 400$ K) and LT ($T = 300$ K) phases (b) along $\bar{M}'$-$\bar{\Gamma}'_{10}$; (c) along the line parallel to $\bar{M}'$-$\bar{\Gamma}'_{10}$ and shifted off by 0.12 Å^{-1}; (d) along $\bar{\Gamma}'_{00}$-$\bar{\Gamma}'_{10}$. The momentum components along the [100] direction, k_x, are indicated.

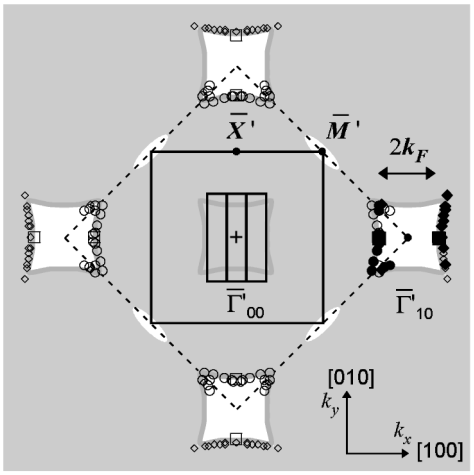

FIG. 3. The FS of the HT phase determined at 400 K. Solid circles denote data taken with $h\nu = 22.78$ eV and $\theta_i = 45°$ in the (110) plane, solid squares with $h\nu = 22.78$ eV and $\theta_i = 45°$ in the (100) plane, and solid diamonds with unpolarized He-II radiation and $\theta_i = 30°$ in the (110) plane. Open symbols are generated by mirror operation. The gray lines enclosing the $\bar{\Gamma}'$ points show FS generated according to the $c(2 \times 2)$ translational symmetry in the extended zone scheme. The solid lines represent SBZ of $c(2 \times 2)$-In (large square) and $(9\sqrt{2} \times 2\sqrt{2})R45°$-In (small rectangles). Also shown is SBZ of Cu(001)-(1×1) with the dashed lines. The shaded region shows the Cu bulk FS projected onto Cu(001)-(1×1) (see text). $\bar{\Gamma}'_{00} - \bar{\Gamma}'_{10} = 1.74$ Å^{-1}.

for each curve, in the unit of Å^{-1}, indicates the momentum component parallel to $\bar{\Gamma}'_{00}$-$\bar{\Gamma}'_{10}$. For the HT phase, the S band approaches E_F with increasing k_x and crosses E_F. On the other hand, for the LT phase the S does not cross E_F but disperses back to higher binding energies, which shows that a large energy gap is formed at E_F in the LT phase. The maximum of the backfolded S band is located ~400 meV below E_F.

Figure 2(c) shows spectra taken along the line parallel to $\bar{M}'$-$\bar{\Gamma}'_{10}$ but shifted off by 0.12 Å^{-1}. The incident conditions are the same as for Fig. 2(b). The Fermi surface crossing at 400 K and the backfolding of the S band at 300 K is discernible also in these data. The energy gap is decreased upon going off the $\bar{M}'$-$\bar{\Gamma}'_{10}$ line. The spectra along $\bar{\Gamma}'_{00}$-$\bar{\Gamma}'_{10}$ are shown in Fig. 2(d). The experimental conditions are the same as those for Figs. 2(b) and 2(c) except that the light is incident in a (100) plane. In this case also, the S band crosses E_F and then disappears for the HT phase. For the LT phase, it is difficult to tell within our energy resolution if the S band crosses the Fermi level. However, a backfolded band is seen at larger k_x dispersing back to higher binding energies.

It is noted that the backfolding points in the LT phase, observed for all the angular scans including those along $\bar{M}'$-$\bar{\Gamma}'_{10}$ [Fig. 2(c)] and $\bar{\Gamma}'_{00}$-$\bar{\Gamma}'_{10}$ [Fig. 2(e)], coincide with a new SBZ boundary of the LT phase, as discussed below.

We traced the S peak throughout a quadrant of (1×1)-SBZ. In order to determine the crossing points against E_F of the S band in the HT phase, we measured many spectra by rotating the analyzer in 0.5°–1.0° interval with the incident conditions fixed. The crossing points were determined by extrapolating the peak position in a series of spectra up to E_F. In Fig. 3, the FS thus determined experimentally from three sets of data, two with synchrotron radiation and one with unpolarized He-II radiation, are shown by solid symbols. The three sets of data are in good agreement. The open symbols in Fig. 3 are generated by symmetry operations corresponding to mirror planes and the gray lines by the translational symmetry operation corresponding to $c(2 \times 2)$. The FS has a squarelike shape and defines hole pockets enclosing $\bar{\Gamma}'$ points. The experimental data plotted along the top and bottom sides of the square are sparse, because of the small photoemission cross section of the S

peak. Note that any In-induced features around $\bar{\Gamma}'_{00}$ could not be observed because of strong and broad photoemission due to the bulk Cu sp band.

Also shown in Fig. 3 is the Cu bulk FS projected onto the (001) surface calculated by an interpolation scheme [15]. Note that the projected FS of bulk Cu is shown for the (1×1) symmetry for comparison's sake and should actually be rearranged for the $c(2 \times 2)$ surface. The projected bulk hole pockets around $\bar{\Gamma}'$ [$\bar{M}$ for (1×1)] disappears for the $c(2 \times 2)$ symmetry, which means that the FS determined for the HT phase is not strictly of 2D nature.

The S band is formed by the interaction of In $5sp$ with the Cu $4sp$ bands. It is hence reasonable to find the square-shaped 2D FS for the HT phase, which mimics the edge of the projected bulk FS of Cu. This is analogous to the cases of clean metal surfaces [4] where the 2D FS of surface localized states resembles the projected bulk FS because the surface states are produced when bulk states are subjected to the perturbation by the surfaces.

In Fig. 3 we find a squarelike FS with large straight sides which is favorable for nesting. In the HT phase the Fermi wave vector, k_F, along [100] and [010] is located at 1.44 Å^{-1} from $\bar{\Gamma}_{00}$ and 0.30 Å^{-1} from $\bar{\Gamma}_{10}$. STM and LEED show that the structure in the LT phase is characterized by the two modulation vectors: $Q_1 = 2\pi/9a_0 = 0.19$ Å^{-1} along [100] and $Q_2 = 2\pi/2a_0 = 0.87$ Å^{-1} along [010]. Neither Q_1 nor Q_2 is consistent with a simple nesting condition, $2k_F = Q$. However, as shown in Fig. 3, the SBZ boundary of the $(9\sqrt{2} \times 2\sqrt{2})R45°$ structure coincides with the FS of the HT phase; $3Q_1$ (0.58 Å^{-1}) is in close agreement with $2k_F$ of the HT phase along [100]. Thus a 1D generalized nesting condition, $Q_1 = 2k_F/3$, holds for this system [2], which leads to the Peierls transition. It is noted that the FS of the HT phase is slightly curved, which may be the reason for the variation of the energy gap: the largest ($2\Delta \sim 800$ meV) at the corners of the square and the smallest at the middle of the sides.

Thus we suggest that the PLD in the LT phase is stabilized by coupling with the charge density modulation, since the energy gap formation accompanied with partial FS nesting reduces the total energy of valence electrons. We, however, have some remaining questions about the mechanism for the transition: First, why are no manifestations of the $2k_F$ effect observed in our experiment? It might be argued that the energy cost in the Cu bands, in the near-surface region, is high for PLD corresponding to $2k_F$. As noted before, the S band is a surface resonance and couples with 3D electronic states of the substrate. On the other hand, the Cu bands should also experience the new periodicity and contribute to the total energy change. The second question is on the origin of the lattice distortion corresponding to Q_2, which cannot be accounted for by the 1D FS nesting mechanism described above. These questions should be addressed in future studies.

In summary, we have studied a reversible phase transition at around 350 K between $c(2 \times 2)$-In and $(9\sqrt{2} \times 2\sqrt{2})R45°$-In on In/Cu(001). STM and LEED demonstrate a strong PLD in the LT phase. The ARPES experiment reveals that this transition is essentially a CDW transition and that a large gap opening occurs in the LT phase by the Peierls mechanism. Hence this system serves a novel quasi-2D system coupled to a 3D electron system, and further study will shed new light on the physics of reduced dimensional materials. Surface crystallographic studies will yield the precise magnitude of PLD, which then will reveal the true charge density modulation.

The synchrotron ARPES experiment has been done under the approval of the Photon Factory Program Advisory Committee (PF-PAC No. 98G226).

*Present address: Institute of Experimental Physics, Johannes Kepler Universität, A-4040 Linz, Austria.
†Present address: School of Advanced Sciences, The Graduate University for Advanced Studies, Kanagawa 240-0193, Japan.
‡Electronic address: aruga@kuchem.kyoto-u.ac.jp

[1] G. Grüner, *Density Waves in Solids* (Addison-Wesley, Reading, MA, 1994).
[2] R. E. Peierls, *Quantum Theory of Solids* (Clarendon, Oxford, 1955).
[3] T. E. Felter, R. A. Barker, and P. J. Estrup, Phys. Rev. Lett. **38**, 1138 (1977); M. K. Debe and D. A. King, Phys. Rev. Lett. **39**, 708 (1977).
[4] K. E. Smith and S. D. Kevan, Phys. Rev. B **43**, 3986 (1991).
[5] K. E. Smith, G. E. Elliott, and S. D. Kevan, Phys. Rev. B **42**, 5385 (1990).
[6] D. Singh and H. Krakauer, Phys. Rev. B **37**, 3999 (1988).
[7] J. M. Carpinelli *et al.,* Nature (London) **381**, 398 (1996).
[8] J. M. Carpinelli *et al.,* Phys. Rev. Lett. **79**, 2859 (1997).
[9] J. Avila *et al.,* Phys. Rev. Lett. **82**, 442 (1999).
[10] A. Mascaraque *et al.,* Phys. Rev. Lett. **82**, 2524 (1999).
[11] H. W. Yeom *et al.,* Phys. Rev. Lett. **82**, 4898 (1999).
[12] P. Heimann *et al.,* Phys. Rev. Lett. **42**, 1782 (1979).
[13] S. D. Kevan, Phys. Rev. B **28**, 2268 (1983).
[14] T. Nakagawa *et al.* (unpublished).
[15] N. V. Smith, Phys. Rev. B **19**, 5019 (1979).